Site-bond percolation on simple cubic lattices: numerical simulation and analytical approach

J. Stat. Mech. (2016) 093210

(http://iopscience.iop.org/1742-5468/2016/9/093210)

Journal of Statistical Mechanics: Theory and Experiment
An IOP and SISSA journal

PAPER: Classical statistical mechanics, equilibrium and non-equilibrium

Site-bond percolation on simple cubic lattices: numerical simulation and analytical approach

M I González[1], P M Centres[1], W Lebrecht[2] and A J Ramirez-Pastor[1]

[1] Departamento de Física, Instituto de Física Aplicada, Universidad Nacional de San Luis-CONICET, Ejército de Los Andes 950, D5700HHW, San Luis, Argentina

[2] Departamento de Ciencias Físicas, Universidad de La Frontera, Casilla 54-D, Temuco, Chile

E-mail: antorami@unsl.edu.ar

Received 13 April 2016, revised 3 July 2016
Accepted for publication 25 August 2016
Published 29 September 2016

Online at stacks.iop.org/JSTAT/2016/093210
doi:10.1088/1742-5468/2016/09/093210

Abstract. The site-percolation problem on simple cubic lattices has been studied by means of numerical simulation and analytical calculations based on exact counting of configurations on finite cells. Motivated by considerations of cluster connectivity, two distinct schemes (denoted as $S \cap B$ and $S \cup B$) have been considered. In $S \cap B$ ($S \cup B$), two points are said to be connected if a sequence of occupied sites *and* (*or*) bonds joins them. Theoretical and numerical results, supplemented by analysis using finite-size scaling theory, were used to calculate the complete phase diagram of the system in the (p_s, p_b) space. Our study allowed us also to determine the critical exponents (and universality) characterizing the phase transition occurring in the system.

Keywords: critical exponents and amplitudes, numerical simulations, percolation problems, phase diagrams

1742-5468/16/093210+17$33.00

Contents

1. Introduction

The site-bond percolation problem and its applications have been studied for a very long time [1–9]. In this scheme, sites and bonds are randomly and independently occupied with occupancy fractions p_s and p_b, respectively. It is possible then to define *site-and-bond* ($S \cap B$) and *site-or-bond* ($S \cup B$) percolation: in $S \cap B$ ($S \cup B$), two points are said to be connected if a sequence of occupied sites *and* (*or*) bonds joins them. Thus, in $S \cap B$, a cluster is considered to be a set of occupied bonds and sites in which the bonds are joined by occupied sites, and the sites are joined by occupied bonds. In $S \cup B$, a bond or site contributes to cluster connectivity independently of the occupation of its endpoints[3]. The central idea of the site-bond percolation theory is based on finding the minimum concentration of elements (sites and bonds) for which a cluster extends from one side to the opposite one of the lattice, and a second order phase transition occurs in the system.

In the case of $S \cap B$ site-bond percolation, the problem has many applications in different fields and has been widely studied (in particular for a square lattice) [10–17]. For instance, it was used to describe the sol-to-gel transition (gelation) of polymers [10]. Thus, the critical curve corresponding to the $S \cap B$ problem separates a percolating regime, in which a gel is formed, from a non-percolating regime, the sol phase.

$S \cap B$ model was mentioned at first by Frisch and Hammersley [11]. Agrawal *et al* [12] and Nakanishi and Reynolds [13] showed, by using a series method and position-space renormalization group, respectively, that the critical exponents of pure site percolation are also valid for site-bond percolation. Later, Yanuka and Englman [14] proposed a

[3] $S \cap B$ and $S \cup B$ models will be explained in details in section 2.1.

J. Stat. Mech. (2016) 093210

equation for the critical curve separating the sol-to-gel transition for square, triangular, simple cubic and face centered cubic (fcc) lattices. Tarasevich and van der Marck [15] presented a very complete and systematic study, where site-bond percolation thresholds were calculated by means of numerical simulations in many lattices in two to five dimensions. Ziff and Gu [16] developed an approximation, which allows the estimation of very accurate thresholds for a wide variety of systems. In addition, an accurate expression for the criticality condition of site-bond percolation on the honeycomb lattice was obtained in [16]. More recently, a correlated bond-site percolation model was introduced by Nduwayo *et al* [17]. In all cases, standard site (bond) percolation is recovered as $p_b = 1$ ($p_s = 1$).

On the other hand, the $S \cup B$ model has received considerably less attention in the literature [18–20]. In particular, the critical curve corresponding to the $S \cup B$ problem on simple cubic lattices has not yet been reported. The main objective of this paper is to provide a thorough study in this direction. For this purpose, extensive computer simulations have been carried out to study the complete site-bond percolation problem on simple cubic lattices. The numerical results, supplemented by analysis using finite-size scaling theory [4, 21, 22], allowed to determine the critical quantities (percolation thresholds and critical exponents) characterizing the phase transition occurring in the system.

Despite the simplicity of its definition, percolation theory (and the evaluation of the corresponding percolation thresholds) has resisted exact calculations. In particular, analytical calculations of thresholds have proven to be a rather difficult task only overcome for a given number of simple geometries. Thus, percolation thresholds are known exactly only for two-dimensional systems. There are no known exact results in three dimensions. Even in two dimensions, there are no exact results for site-bond percolation on regular lattices. In this line, a cluster-exact approximation was presented in a recent paper from our group [23]. This theoretical approach is based on the exact calculation of configurations on finite cells, and its extrapolation to larger system sizes.

Cluster-exact calculations proved to be a very useful tool for the research of percolation on square lattices [23–25]. The results showed, in addition, that the technique could be also applied to study percolation on triangular lattices [20]. Here, the scheme introduced in Ref. [23] is extended to include three-dimensional (3D) lattices. For this purpose, finite $L_x \times L_y \times L_z$ cells are used to calculate the complete phase diagram in the (p_s, p_b) space for sites and bonds independently and randomly deposited on a simple cubic lattice. The study is a natural continuation of our previous work [20, 23–25], and complement the numerical analysis.

The paper is organized as follows. The model and the simulation scheme are described in section 2. The theoretical approach is introduced in section 3, which includes the main results concerning the phase diagrams obtained from the analytical calculations. Details of the calculations are given in the appendix. The conclusions are drawn in section 4.

2. Model and simulation scheme

2.1. The model

Let us consider an initially empty simple cubic lattice of $M = L_x \times L_y \times L_z$ size and open boundary conditions. Sites and bonds are independently and randomly deposited with

J. Stat. Mech. (2016) 093210

concentrations p_s and p_b, respectively. The filling process is as follows: (1) a given site (bond), belonging to the set of empty sites (bonds), is randomly selected and occupied; and (2) the set of empty sites (bonds) is updated. The procedure (1) and (2) is repeated until N_s sites and N_b bonds are occupied, and the desired concentrations ($p_s = N_s/M$, $p_b = N_b/3M$) are reached.

The $S \cap B$ model can be considered as a correlated bond percolation problem, or a pure site problem in which one replaces the bond by a site with two neighbors. On the other hand, the $S \cup B$ model can also be thought of as a bond problem, but not seem to be expressible as a pure site problem. Then, in order to calculate the percolation threshold, we can now think of a mapping $\mathbf{L} \to \mathbf{L}'$ from the original site-bond lattice $\mathbf{L}$ to an effective bond lattice $\mathbf{L}'$ where each bond and its endpoints sites of $\mathbf{L}$ transforms into a bond one of $\mathbf{L}'$. The rules for the mapping depend on the studied problem. Thus, for *site-and-bond* percolation:

(i) each empty bond of $\mathbf{L}$ transforms into an empty one of $\mathbf{L}'$;

(ii) each occupied bond with one or two empty endpoint sites of $\mathbf{L}$ transforms into an empty bond in $\mathbf{L}'$; and

(iii) each occupied bond with its occupied endpoint sites of $\mathbf{L}$ transforms into an occupied bond of $\mathbf{L}'$

On the other hand, for *site-or-bond* percolation:

(i) each occupied bond of $\mathbf{L}$ transforms into an occupied bond one of $\mathbf{L}'$;

(ii) each empty bond with one or two empty endpoint sites of $\mathbf{L}$ transforms into an empty bond in $\mathbf{L}'$; and

(iii) each empty bond with its occupied endpoint sites of $\mathbf{L}$ transforms into an occupied bond of $\mathbf{L}'$.

Once the mapping is completed, each percolating/non-percolating configuration in the effective lattice corresponds to a percolating/non-percolating configuration in the original lattice. Then, the standard Hoshen and Kopelman algorithm [26] was applied for studying bond percolation on $\mathbf{L}'$. The positions of the deposited objects were generated by using the Mersenne twister random number generator [27].

2.2. Simulation results

It is well-known that it is quite a difficult matter to analytically determine the value of a percolation threshold for a given lattice [4]. For some special types of lattice, geometrical considerations enable their percolation thresholds to be derived exactly. For different conditions, i.e. for systems which do not present such a topological advantage, percolation thresholds have to be estimated numerically by means of computer simulations.

In the present case, each simulation run consists of the following three steps: (a) the construction of the simple cubic lattice (with $L_x = L_y = L_z = L$) for the desired fractions p_s and p_b of sites and bonds, respectively; (b) the mapping from the original site-bond

J. Stat. Mech. (2016) 093210

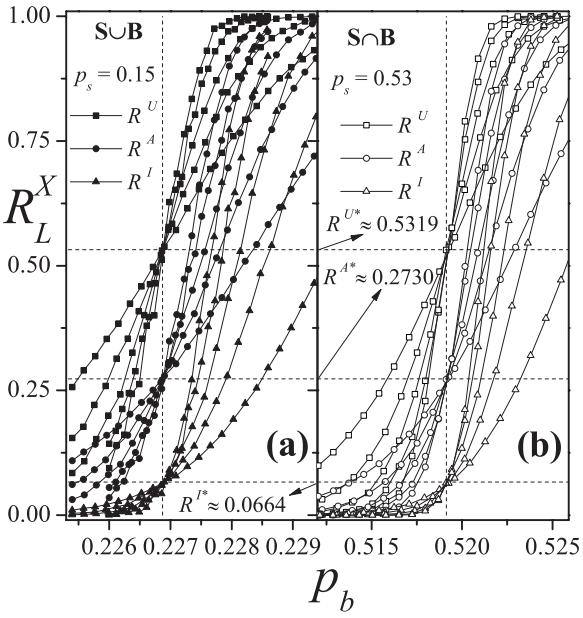

Figure 1. Fraction of percolating lattices R_L^X ($X = I,\ U,\ A$ as indicated) as a function of the bond concentration p_b for two typical cases: (a) $S \cup B$ model and $p_s = 0.15$; and (b) $S \cap B$ model and $p_s = 0.53$. For each criterion, different lattice sizes were considered ($L = 96$,144, 192, 240, 288). Horizontal dashed lines show the R^{X^*} universal points. Vertical dashed lines denote the percolation thresholds $p_{b,c}$ in the thermodynamic limit $L \to \infty$.

lattice to the effective bond lattice; and (c) the cluster analysis by using the Hoshen and Kopelman algorithm [26] on the effective bond lattice. In the last step, the existence of a percolating island is verified. For this purpose, the probability $R_L^X(p_s, p_b)$ that a lattice composed of $L \times L \times L$ sites percolates at the concentration (p_s, p_b) can be defined. Here, the following definitions can be given according to the meaning of X [21]:

- $R_L^R(p_s, p_b)$: the probability of finding a rightward percolating cluster, along the x-direction,
- $R_L^F(p_s, p_b)$: the probability of finding a frontward percolating cluster, along the y-direction,
- $R_L^D(p_s, p_b)$: the probability of finding a downward percolating cluster, along the z-direction.

Other useful definitions for the finite-size analysis are:

- $R_L^U(p_s, p_b)$: the probability of finding a cluster which percolates on any direction,
- $R_L^I(p_s, p_b)$: the probability of finding a cluster which percolates in the three (mutually perpendicular) directions,
- $R_L^A(p_s, p_b) = \frac{1}{3}[R_L^R(p_s, p_b) + R_L^F(p_s, p_b) + R_L^D(p_s, p_b)]$.

doi:10.1088/1742-5468/2016/09/093210

J. Stat. Mech. (2016) 093210

A total of m_L independent runs of such three steps are carried out for obtaining the number m_L^X of them for which a percolating cluster of the desired criterion X is found. Then, $R_L^X(p_s, p_b) = m_L^X/m_L$ is defined. In the present study, a set of $m_L = 5 \times 10^5$ independent samples are numerically prepared for each model ($S \cup B$ and $S \cap B$), for each pair (p_s, p_b) and lattice size L ($L = 96$, 144, 192, 240, 288). From the point of view of calculations, we set $p_s =$ constant and vary p_b.

In figure 1, the probabilities R_L^I (triangles), R_L^U (squares) and R_L^A (circles) are presented for two typical cases: (a) $S \cup B$ percolation and $p_s = 0.15$; and (b) $S \cap B$ percolation and $p_s = 0.53$. As already explained, p_b is varied during the simulation process.

From a simple inspection of figure 1 (and from data not shown here for a sake of clarity), it is observed that R_L^X curves cross each other in a unique point R^{X^*}. The value of R^{X^*} depends on the criterion X used: $R^{A^*} \approx 0.2730$; $R^{I^*} \approx 0.0664$ and $R^{U^*} \approx 0.5319$. In addition, the crossing points do not modify their numerical value for the different studied cases, as a first indication that the problem belongs to the same universality class no matter the model ($S \cup B$ or $S \cap B$) and the value of p_s used in the experiment.

In order to express $R_L^X(p_s, p_b)$ as a function of continuous values of p_b, it is convenient to fit $R_L^X(p_s, p_b)$ with some approximating function through the least-squares method. The fitting curve is the *error function* because $\mathrm{d}R_L^X/\mathrm{d}p_b$ is expected to behave like the Gaussian distribution[4]

$$\frac{\mathrm{d}R_L^X}{\mathrm{d}p_b} = \frac{1}{\sqrt{2\pi}\,\Delta_L^X} \exp\left\{-\frac{1}{2}\left[\frac{p_b - p_{b,c}^X(L)}{\Delta_L^X}\right]^2\right\}, \tag{1}$$

where $p_{b,c}^X(L)$ is the concentration at which the slope of $R_L^X(p_s, p_b)$ is the largest and Δ_L^X is the standard deviation from $p_{b,c}^X(L)$.

The standard theory of finite-size scaling [4] allows for various efficient routes to estimate the critical exponent ν from simulation data. One of these methods is from the maximum of the function in equation (A.1),

$$\left(\frac{\mathrm{d}R_L^X}{\mathrm{d}p_b}\right)_{\max} \propto L^{1/\nu}. \tag{2}$$

In figure 2, $\ln[(\mathrm{d}R_L^A/\mathrm{d}p_b)_{\max}]$ has been plotted as a function of $\ln[L]$ (note the log–log functional dependence) for the same cases in figure 1. According to equation (A.2) the slope of each line corresponds to $1/\nu$. As it can be observed, the slopes of the curves remain constant. Thus, $\nu = 0.8756(7)$ for part (a) and $\nu = 0.8767(7)$ for part (b).

Another alternative way for evaluating ν is from the divergence of the root mean square deviation of the threshold observed from their average values, Δ_L^X,

$$\Delta_L^X \propto L^{-1/\nu}. \tag{3}$$

[4] Even though the behavior of $\mathrm{d}R_L^X/\mathrm{d}p_b$ is not a Gaussian function in all of the range of p_b, this quantity is approximately Gaussian near the peak, and equation (A.1) is a good approximation for the purpose of locating its maximum [28].

J. Stat. Mech. (2016) 093210

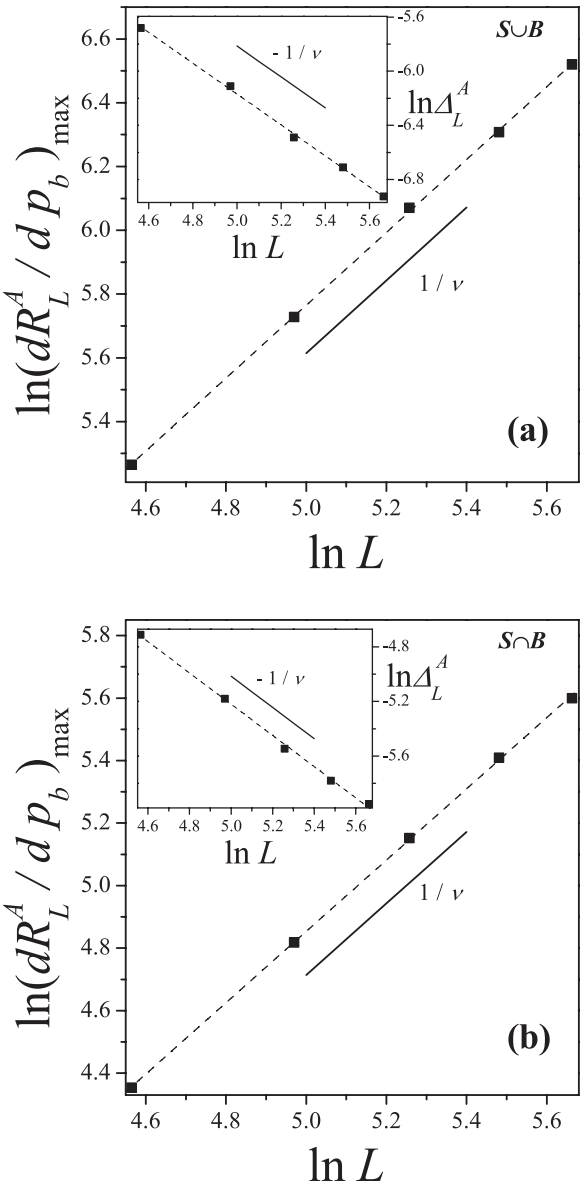

Figure 2. (a) Ln–ln plot of $(\mathrm{d}R_L^A/\mathrm{d}p_b)_{\max}$ as a function of L for the $S \cup B$ model and $p_s = 0.15$. According to equation (A.2) the slope of the curve corresponds to $1/\nu$. Inset: $\ln \Delta_L^A$ as a function of L for the same case in the main figure. According to equation (A.3), the slope of the curve corresponds to $-1/\nu$. (b) As part (a) for the $S \cap B$ model and $p_s = 0.53$.

As an example of the validity of the last equation, the insets in figure 2 shows Δ_L^A as a function of L (note the log–log scale) for the same cases in the main figure. According to equation (A.3), the slope of the line corresponds to $-1/\nu$. In this case, $\nu = 0.8761(9)$, part (a) and $\nu = 0.8757(8)$ part (b).

The study in figure 2 was repeated for different values of p_s and the I, U and A criteria. In all cases, the results obtained for ν coincide, within numerical errors, with the previously reported values for the ordinary 3D percolation [29–33] (see Wikipedia webpage: https://en.wikipedia.org/wiki/Percolation_critical_exponents).

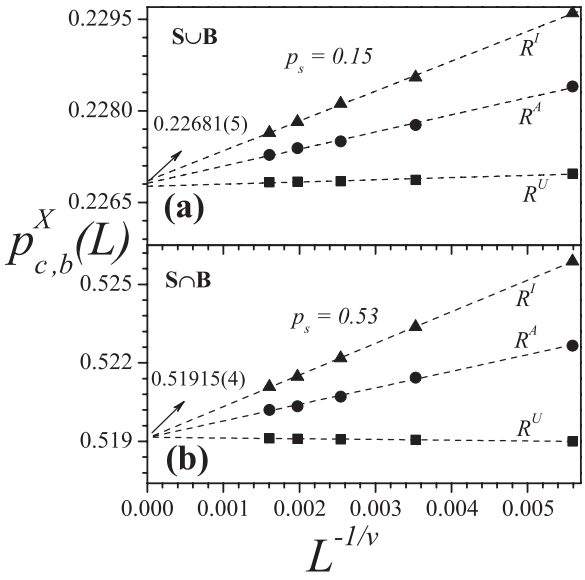

Figure 3. Extrapolation of $p^X_{c,b}(L)$, towards the thermodynamic limit according to the theoretical prediction given by equation (A.4). Triangles, circles and squares denote the values of $p^X_{c,b}(L)$, obtained by using the criteria I, A and U, respectively. (a) $S \cup B$ model and $p_s = 0.15$. (b) $S \cap B$ model and $p_s = 0.53$.

Once ν is known, the percolation threshold $p_{b,c}$ can be obtained from the extrapolation of the positions $p^X_{b,c}(L)$ of the maxima of the slopes of $R^X_L(p_s, p_b)$. For each criterion (I, U and A), for each percolation model ($S \cup B$ and $S \cap B$) and for each value of p_s, one expects that [4],

$$p^X_{b,c}(L) = p_{b,c} + A^X L^{-1/\nu}, \tag{4}$$

where A^X is a non-universal constant and ν will taken as 0.8760.

Figure 3 shows the plots towards the thermodynamic limit of $p^X_{b,c}(L)$ according to equation (A.4) for the data in figures 1 and 2. From extrapolations it is possible to obtain the percolation thresholds for the criteria I, A and U. Combining the three estimates for each case, the final values of $p_{b,c}$ can be obtained. Additionally, the maximum of the differences between $|p^U_{b,c} - p^A_{b,c}|$ and $|p^I_{b,c} - p^A_{b,c}|$ gives the error bar for each determination of $p_{b,c}$. In this case, the values obtained were: $p_{b,c} = 0.226\,81(5)$ (a), and $p_{b,c} = 0.519\,15(4)$ (b).

The scaling behavior can be further tested by plotting R^X_L versus $(p_b - p_{b,c})L^{\frac{1}{\nu}}$ and looking for data collapsing. Using the values of $p_{b,c}$ and ν previously calculated, an excellent scaling collapse was obtained for R^A_L (see figure 4). This leads to independent control and consistency check of numerical value of the critical exponent ν.

J. Stat. Mech. (2016) 093210

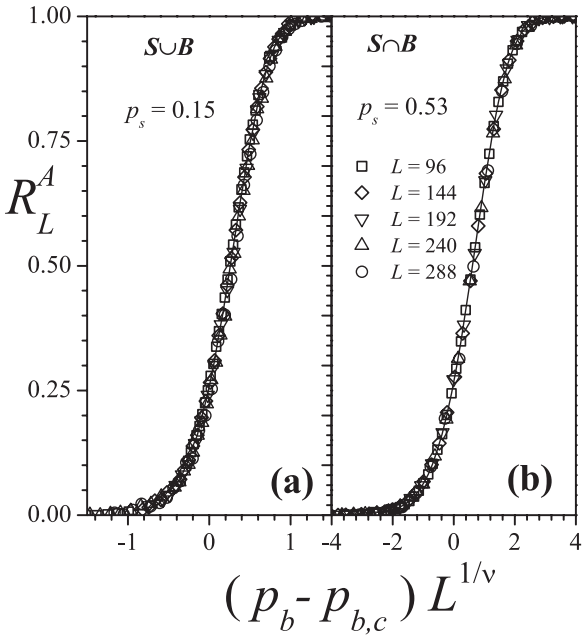

Figure 4. Data collapsing of the fraction of percolating samples R_L^A as a function of the argument $(p_b - p_{b,c})L^{\frac{1}{\nu}}$ for the curves in figure 1. The plots were made using $p_{b,c} = 0.226\,81$ (part (a)), $p_{b,c} = 0.519\,15$ (part (b)), and the percolation exponent $\nu = 0.8760$.

Table 1. Numerical values of (p_s, p_b) for the critical line corresponding to the $S \cup B$ percolation model.

p_s	p_b
0	0.248 811 85(10) [33]
0.075	0.243 72(4)
0.15	0.226 81(5)
0.23	0.184 58(5)
0.27	0.144 69(6)
0.29	0.109 38(4)
0.30	0.084 42(5)
0.31	0.033 34(5)
0.311 607 68(15) [33]	0

Note: Error estimates concerning the last digit are indicated between brackets.

The procedure in figure 3 was is repeated for different values of p_s. The results, which are collected in tables 1 and 2, represent the complete phase diagram of the system in the (p_s, p_b) space. In section 3.2, the simulation data obtained in the present section will be discussed in comparison with cluster-exact calculations and previous studies in the literature [15].

J. Stat. Mech. (2016) 093210

Table 2. Numerical values of (p_s, p_b) for the critical line corresponding to the $S \cap B$ percolation model.

p_s	p_b
0.311 607 68(15) [33]	1
0.33	0.922 82(6)
0.37	0.796 27(5)
0.41	0.699 24(6)
0.47	0.599 85(4)
0.53	0.519 15(4)
0.65	0.407 38(5)
0.75	0.344 72(6)
0.85	0.299 76(5)
0.95	0.263 45(5)
1	0.248 811 85(10) [33]

Note: Error estimates concerning the last digit are indicated between brackets.

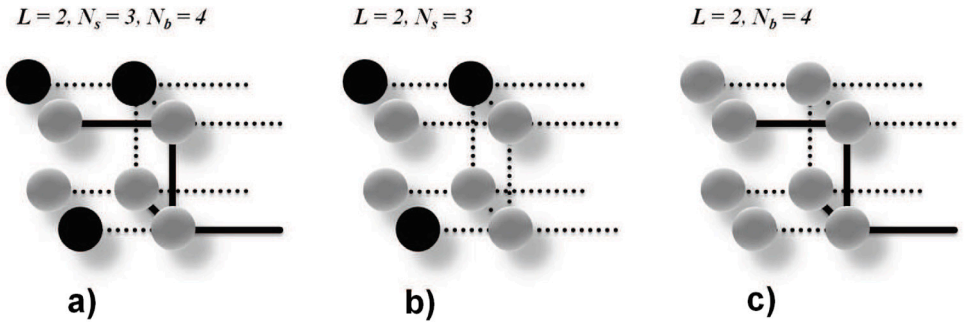

Figure 5. (a) Snapshot corresponding to a $2 \times 2 \times 2$ cell with three occupied sites ($N_s = 3$) and four occupied bonds ($N_b = 4$). Black circles, gray circles, solid lines and dotted lines represent occupied sites, empty sites, occupied bonds and empty bonds, respectively. (b) Site lattice corresponding to the configuration shown in part (a). (c) Bond lattice corresponding to the configuration shown in part (a).

3. Analytical approximation and comparison between simulation and theoretical results

3.1. The theoretical approach: exact calculations of configurations on finite cells

The theoretical approach is based on exact calculations of configurations [20, 23–25] with the following assumptions: (i) the original system is divided into separate site and bond problems that are independently analyzed (see figure 5); (ii) the percolation is measured along the x-axis; and (iii) symmetric $L_x = L_y = L_z = L$ cells are used in the calculations. The percolation trajectory ℓ is defined as the number of objects belonging to the percolating cluster. Thus, the minimum percolation trajectory, represented by $\ell_{\min}$, corresponds to the direct percolation path from left to right (or vice versa), being $\ell_{\min} = L_x$ for sites and bonds. On the other hand, the maximum percolation trajectory, represented by $\ell_{\max}$, corresponds to the number of objects in the saturated cell, being $\ell_{\max} = L_x L_y L_z$ and $L_x L_y L_z + (L_x - 1)(L_y - 1)L_z + L_y(L_x - 1)(L_z - 1)$ for sites and bonds,

J. Stat. Mech. (2016) 093210

respectively (see figure 5). In general, the length of a percolation trajectory varies between $\ell_{\min}$ and $\ell_{\max}$.

In the case of sites, the percolation probability of for any given cell includes the addition of the individual probabilities of all percolating trajectories leading to a polynomial function $f(p_s)$, where $\ell_{\min} = L_x$ determines the minimum degree of the polynomial function, and $\ell_{\max} = L_xL_yL_z$ corresponds to the maximum degree associated to it. Then,

$$f(p_s) = \sum_{\ell=\ell_{\min}}^{\ell_{\max}} C_\ell^s \, p_s^\ell (1-p_s)^{\ell_{\max}-\ell}, \tag{5}$$

where the coefficients C_ℓ^s's correspond to the totality of the site trajectories of length ℓ leading to percolation. For a $2 \times 2 \times 2$ cell, equation (A.5) results

$$f(p_s) = 4p_s^2 - 6p_s^4 + 4p_s^6 - p_s^8. \tag{6}$$

In the case of bonds, the corresponding polynomial function $g(p_b)$ can be written as

$$g(p_b) = \sum_{\ell=\ell_{\min}}^{\ell_{\max}} C_\ell^b \, p_b^\ell (1-p_b)^{\ell_{\max}-\ell}, \tag{7}$$

where $\ell_{\min} = L_x$, $\ell_{\max} = L_xL_yL_z + (L_x-1)(L_y-1)L_z + L_y(L_x-1)(L_z-1)$ and C_ℓ^b's correspond to the totality of the bond trajectories of length ℓ leading to percolation. For a $2 \times 2 \times 2$ cell, equation (A.7) results

$$g(p_b) = 4p_b^2 + 8p_b^3 - 14p_b^4 - 40p_b^5 + 16p_b^6 + 228p_b^7 - 665p_b^8 + 672p_b^9 - 376p_b^{10} + 112p_b^{11} - 14p_b^{12}. \tag{8}$$

Once $f(p_s)$ and $g(p_b)$ are obtained, the percolation functions corresponding to $S \cap B$ and $S \cup B$ site-bond percolation are calculated by following the Tsallis scheme [34],

$$h_{S\cap B}(p_s, p_b) = f(p_s)g(p_b) \tag{9}$$

and

$$h_{S\cup B}(p_s, p_b) = f(p_s) + g(p_b) - f(p_s)g(p_b). \tag{10}$$

Equations (9) and (10) allow us to obtain the exact percolation functions corresponding to $S \cap B$ and $S \cup B$ problems from the exact percolation functions corresponding to pure site percolation ($f(p_s)$) and pure bond percolation ($g(p_b)$). Interested readers are referred to [34] (p 720) for a more complete description of the Tsallis scheme. Then, for a $2 \times 2 \times 2$ cell,

$$\begin{aligned} h_{S\cap B}(p_s, p_b) = {} & (4p_s^2 - 6p_s^4 + 4p_s^6 - p_s^8)(4p_b^2 + 8p_b^3 - 14p_b^4 - 40p_b^5 + 16p_b^6 + 228p_b^7 - 665p_b^8 + \\ & 672p_b^9 - 376p_b^{10} + 112p_b^{11} - 14p_b^{12}). \end{aligned} \tag{11}$$

and

$$\begin{aligned} h_{S\cup B}(p_s, p_b) = {} & (4p_s^2 - 6p_s^4 + 4p_s^6 - p_s^8) + (4p_b^2 + 8p_b^3 - 14p_b^4 - 40p_b^5 + 16p_b^6 + 228p_b^7 \\ & -665p_b^8 + 672p_b^9 - 376p_b^{10} + 112p_b^{11} - 14p_b^{12}) \\ & -(4p_s^2 - 6p_s^4 + 4p_s^6 - p_s^8)(4p_b^2 + 8p_b^3 - 14p_b^4 - 40p_b^5 + 16p_b^6 + 228p_b^7 \\ & -665p_b^8 + 672p_b^9 - 376p_b^{10} + 112p_b^{11} - 14p_b^{12}). \end{aligned} \tag{12}$$

J. Stat. Mech. (2016) 093210

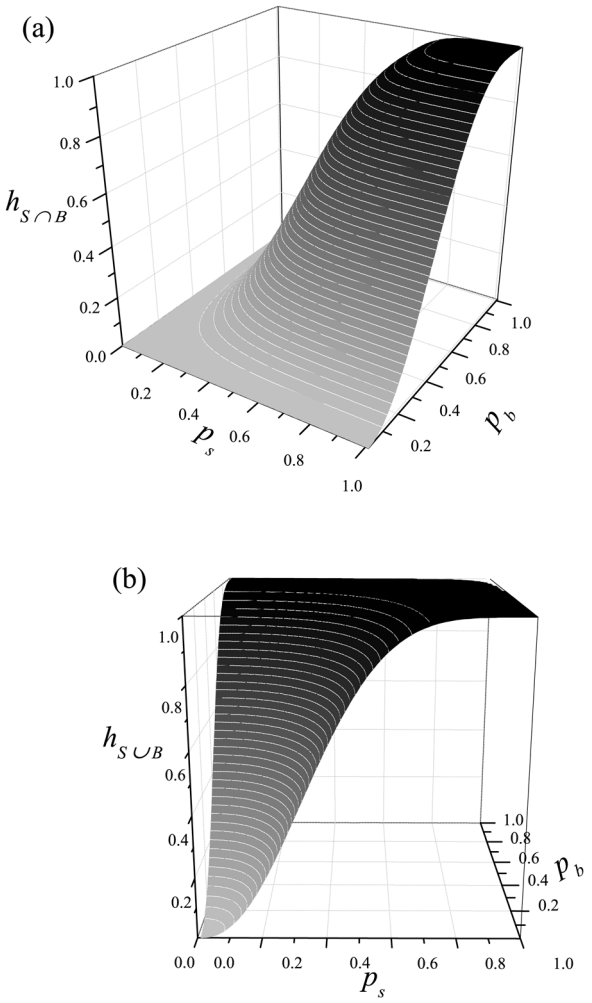

Figure 6. (a) Percolation function $h_{S\cap B}(p_s, p_b)$ (equation (11)) as a function of p_s and p_b. (b) Same as part (a) for $h_{S\cup B}(p_s, p_b)$ (equation (12)).

$h_{S\cap B}(p_s, p_b)$ (equation (11)) and $h_{S\cup B}(p_s, p_b)$ (equation (12)) are plotted in figures 6(a) and (b), respectively. These functions are necessary in order to obtain the critical curves separating the percolating and non-percolating regions ($p_s - p_b$ phase diagram). For this purpose, the string method [35, 36] was used. The procedure is described in the Appendix, and the results are shown in figure 7 (solid lines) in comparison with simulation results (tables 1 and 2) and previous work in the literature [15]. A complete analysis of figure 7 will be performed in the next section.

3.2. Comparison between simulation and theoretical results

Figure 7 shows the comparison between simulation results (solid circles), cluster-exact calculations (solid lines) and data obtained in [15] (crosses) for the complete site-bond percolation phase diagram corresponding to simple cubic lattices.

In the case of $S\cap B$ model, the critical curve separating the percolating and non-percolating regions varies between the point $[p_s = 1.0, p_b = 0.248\,811\,85(10)]$ at left, and the point $[p_s = 0.311\,607\,68(15), p_b = 1.0]$ at right. $p_b = 0.248\,811\,85(10)$ [33]

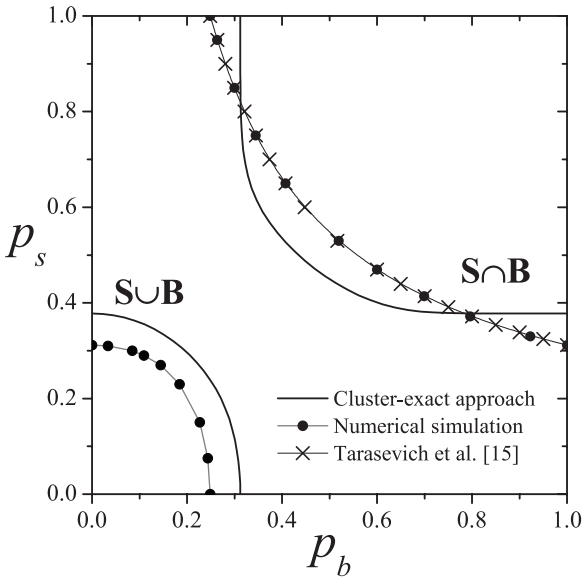

Figure 7. Phase diagrams of site-bond percolation for a simple cubic lattice. Solid circles joined by lines represent simulation results (tables 1 and 2), solid lines correspond to cluster-exact calculations and crosses denote previous data in the literature [15].

Table 3. Cluster-exact calculations for different cell sizes as indicated.

	$S \cup B [S \cap B]$			
Cell size	p_s	p_b	p_s	p_b
$2 \times 2 \times 2$	0 [0.3780(1)]	0.3122(1) [1]	0.3780(1) [1]	0 [0.3122(1)]
$2 \times 2 \times 3$	0 [0.3683(1)]	0.3023(1) [1]	0.3683(1) [1]	0 [0.3023(1)]
$2 \times 3 \times 3$	0 [0.3643(1)]	0.2964(1) [1]	0.3643(1) [1]	0 [0.2964(1)]
$3 \times 3 \times 3$	0 [0.3630(1)]	… … [1]	0.3630(1) [1]	0[… …]
$3 \times 3 \times 4$	0 [0.3594(1)]	… … [1]	0.3594(1) [1]	0[… …]
$\infty \times \infty \times \infty$	0 [0.311 607 68(15)]	0.248 811 85(10) [1]	0.311 607 68(15) [1]	0 [0.248 811 85(10)]

[$p_s = 0.311\,607\,68(15)$ [33] represents the percolation threshold for the standard bond [site] percolation on a simple cubic lattice. An extensive list of percolation thresholds for $d \in [2, 13]$ (d is the dimension of the space) can be found on the Wikipedia webpage: https://en.wikipedia.org/wiki/Percolation_threshold.

As it can be observed from the upper right part of figure 7, the simulation results obtained in the present work (solid circles joined by lines) coincide, within numerical errors, with the results reported by Tarasevich and van der Marck [15] (crosses). The excellent agreement between our data and previous studies supports the applicability of the methodology used in the present paper.

On the other hand, the line of threshold values corresponding to the $S \cup B$ percolation model varies between the point [$p_s = 0.311\,607\,68(15), p_b = 0.0$] at left, and the point [$p_s = 0.0, p_b = 0.248\,811\,85(10)$] at right. In this case, the $S \cup B$ critical curve is reported for the first time in the present study.

As mentioned above, standard site (bond) percolation is recovered as the $p_b = 1.0$ ($p_s = 1.0$) case of the $S \cap B$ problem, as well as $p_b = 0$ ($p_s = 0$) case of the $S \cup B$ problem. As a consequence of this, the $S \cup B$ critical curve is essentially a continuation of the $S \cap B$ curve (if it is wrapped around the diagram).

With respect to the cluster-exact calculations, the curves shown in the figure were obtained for a $2 \times 2 \times 2$ cell. Despite the small size of the cluster, a good qualitative agreement is obtained between simulation and analytical data. A more accurate determination of the critical curves should require extensive numerical calculations with systems of larger sizes. As a proof of this hypothesis, the endpoints of the $S \cup B$ and $S \cap B$ critical lines were calculated for different values of L_x, L_y, L_z. The results, compiled in table 3, (1) clearly indicate that the accuracy of the cluster calculations improves with increase in the cell size; and (2) support the usefulness of this theoretical approach to be used in the context of lattice percolation problems.

4. Conclusions

Numerical simulation and a cluster-exact approximation have been used to study the site-bond percolation problem on 3D simple cubic lattices. The theoretical formalism is based on exact calculations of configurations on a finite cell. Two distinct schemes, *site-and-bond* ($S \cap B$) and *site-or-bond* ($S \cup B$), have been considered. In $S \cap B$, a cluster is considered to be a set of occupied bonds and sites in which the bonds are joined by occupied sites, and the sites are joined by occupied bonds. In $S \cup B$, a bond or site contributes to cluster connectivity independently of the occupation of its endpoints.

The numerical data, supplemented by analysis using finite-size scaling theory, were used to calculate the complete phase diagram of the system in the (p_s, p_b) space. In the $S \cap B$ case, the results coincide with previous reports [15]. In the $S \cup B$ case, the critical line separating the percolating and non-percolating regions is presented for the first time in the literature. In addition, the accurate determination of the critical exponent ν indicates that, in all cases, the problem belongs to the universality class of 3D random percolation.

The simulation results were compared with analytical calculations based on exact counting of configurations on finite $L_x \times L_y \times L_z$ cells. The theoretical scheme is simple, mathematically handleable, and provides results in a good qualitative agreement with the simulation data.

Acknowledgments

WL thanks support from Dirección de Investigación Universidad de La Frontera (Chile), under project DIUFRO No DI 15-0011. MIG, PMC and AJR-P thank support from Universidad Nacional de San Luis (Argentina) under project 322000, CONICET (Argentina) under project PIP 112-201101-00615 and the National Agency of Scientific and Technological Promotion (Argentina) under project PICT-2013-1678. MIG would like to thank M S Nazzarro for his collaboration. The calculations were carried out using (1) the supercomputing infrastructure of the NLHPC (ECM-02) at Centro de

J. Stat. Mech. (2016) 093210

Excelencia en Modelación y Computación Científica at Universidad de La Frontera CEMCC-UFRO, Chile; and (2) the BACO2 parallel cluster located at Instituto de Física Aplicada, CONICET-Universidad Nacional de San Luis, Argentina.

Appendix

As indicated in section 3.1, $h_{S\cap B}(p_s, p_b)$ and $h_{S\cup B}(p_s, p_b)$ are obtained using the Tsallis scheme [34] and the explicit forms of $f(p_s)$ and $g(p_b)$. See equations (A.5)–(12).

Once the functions $h_{S\cap B}(p_s, p_b)$ and $h_{S\cup B}(p_s, p_b)$ are determined, the projections of these surfaces on the planes (p_b = constant) and (p_s = constant) behave in a similar way to the curves of the percolation order parameter obtained with respect to one variable while keeping the second constant. Accordingly, the mentioned projections show a change in the concavity (inflection points), which can be associated to the existence of a transition from a non-percolating to a percolating state.

A way to study the local curvature of $h_{S\cap B}(p_s, p_b)$ and $h_{S\cup B}(p_s, p_b)$ is by using the concept of gradient. Thus,

$$\begin{aligned}\vec{\nabla} h_{S\cap B}(p_s,p_b) &= \frac{\partial h_{S\cap B}(p_s,p_b)}{\partial p_s}\widehat{p_s} + \frac{\partial h_{S\cap B}(p_s,p_b)}{\partial p_b}\widehat{p_b} \\ &= \left[g(p_b)\frac{\partial f(p_s)}{\partial p_s}\right]\widehat{p_s} + \left[f(p_s)\frac{\partial g(p_b)}{\partial p_b}\right]\widehat{p_b};\end{aligned} \tag{A.1}$$

$$\begin{aligned}\vec{\nabla} h_{S\cup B}(p_s,p_b) &= \frac{\partial h_{S\cup B}(p_s,p_b)}{\partial p_s}\widehat{p_s} + \frac{\partial h_{S\cup B}(p_s,p_b)}{\partial p_b}\widehat{p_b} \\ &= \left[\frac{\partial f(p_s)}{\partial p_s} - g(p_b)\frac{\partial f(p_s)}{\partial p_s}\right]\widehat{p_s} + \left[\frac{\partial g(p_b)}{\partial p_b} - f(p_s)\frac{\partial g(p_b)}{\partial p_b}\right]\widehat{p_b}.\end{aligned} \tag{A.2}$$

Now, the modulus of the gradients $\|\vec{\nabla} h_{S\cap B}(p_s,p_b)\|$ and $\|\vec{\nabla} h_{S\cup B}(p_s,p_b)\|$ can be calculated as:

$$S_{S\cap B} = \|\vec{\nabla} h_{S\cap B}(p_s,p_b)\| = \sqrt{\left[g(p_b)\frac{\partial f(p_s)}{\partial p_s}\right]^2 + \left[f(p_s)\frac{\partial g(p_b)}{\partial p_b}\right]^2}; \tag{A.3}$$

and

$$S_{S\cup B} = \|\vec{\nabla} h_{S\cup B}(p_s,p_b)\| = \sqrt{\left[\frac{\partial f(p_s)}{\partial p_s} - g(p_b)\frac{\partial f(p_s)}{\partial p_s}\right]^2 + \left[\frac{\partial g(p_b)}{\partial p_b} - f(p_s)\frac{\partial g(p_b)}{\partial p_b}\right]^2}. \tag{A.4}$$

$S_{S\cap B}$ and $S_{S\cup B}$ are shown in figures A1(a) and (b), respectively. As it can be observed, the curves for a fixed value of p_b present a maximum for a given value of p_s, and in the same manner, the curves for a fixed value of p_s present a maximum for a given value of p_b. The set of such maxima can be calculated by the string method [35, 36]. The basic idea of the string method is to find a path of critical points that connect the minimum of the function $V(p_s, p_b) = -S_{S\cap B(S\cup B)}(p_s, p_b)$ by evolution of a string of initial points.

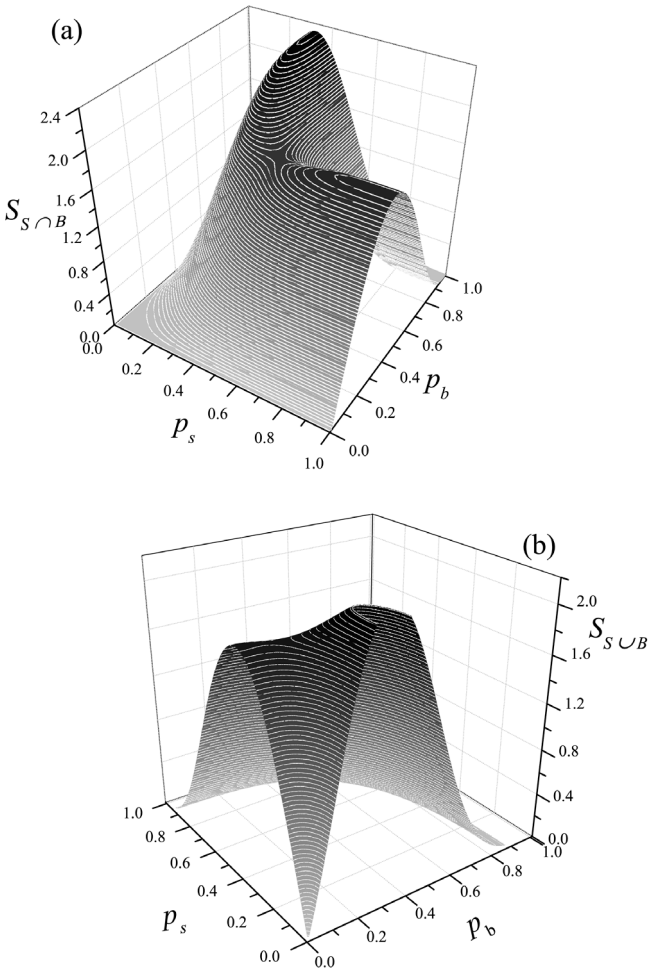

Figure A1. (a) $S_{S\cap B}$ and (b) $S_{S\cup B}$ which are given by equations (A.3) and (A.4) as a function of p_s and p_b.

The string $\{\varphi := (x_i, y_i) \in [0,1], i = 0, 1, 2, ..., n-1\}$ is discretized into $n = 30$ initial points and it evolves until it meets the condition $\vec{\nabla} V(x_i, y_i)^{\perp} = 0$. Where $\vec{\nabla} V(x_i, y_i)^{\perp}$ is the component of $\vec{\nabla} V(x_i, y_i)$ normal to φ, defined the following way

$$\vec{\nabla} V(x_i, y_i)^{\perp} = \vec{\nabla} V(x_i, y_i) - (\vec{\nabla} V(x_i, y_i) \cdot \hat{t})\hat{t}. \tag{A.5}$$

Here $\hat{t}$ denotes the unit tangent of the curve φ and $\cdot$ denotes the Euclidean inner product. Each point of the curve in evolution moves in the direction of the normal component $\vec{\nabla} V(x_i, y_i)$ and the tangential component only moves the points along the string maintaining the spacing between them. Then, the points are redistributed in every movement. The iteration of the method consists in two steps defined as:

(1) Each point of the string initial evolves according to the recurrence equation:

$$x_{i+1} = x_i - \Delta t \frac{\partial V(x_i, y_i)}{\partial p_s}. \tag{A.6}$$

$$y_{i+1} = y_i - \Delta t \frac{\partial V(x_i, y_i)}{\partial p_b}. \tag{A.7}$$

(2) The points along the string are redistributed using a cubic interpolation of the points of the part of the string calculated in each time step Δt.

Finally, when the two endpoints of the initial string fall in the two minimum points of the function $V(p_s, p_b)$, these points are identified. Then, the critical line is obtained from the path of minimum critical points joining the two minimum endpoints. The resulting critical curves are shown as solid lines in figure 7.

References

[1] Broadbent S R and Hammersley J M 1957 *Proc. Camb. Phil. Soc.* **53** 629
Hammersley J M 1957 *Proc. Camb. Phil. Soc.* **53** 642
[2] Kesten H 1982 *Percolation Theory for Mathematicians* (Boston: Birkhäuser)
[3] Zallen R 1983 *The Physics of Amorphous Solids* (New York: Wiley)
[4] Stauffer D and Aharony A 1985 *Introduction to Percolation Theory* 2nd edn (London: Taylor & Francis)
[5] Sahimi M 1994 *Applications of Percolation Theory* (London: Taylor & Francis)
Sahimi M 1995 *Flow and Transport in Porous Media and Fractured Rock* (New York: VCH)
[6] Grimmett G 1999 *Percolation* (Berlin: Springer)
[7] Bollobás B and Riordan O 2006 *Percolation* (New York: Cambridge University Press)
[8] Tarasevich Y Y, Lebovka N I and Laptev V V 2012 *Phys. Rev.* E **86** 061116
[9] Tarasevich Y Y, Laptev V V, Vygornitskii N V and Lebovka N I 2015 *Phys. Rev.* E **91** 012109
[10] Coniglio A, Stanley H E and Klein W 1979 *Phys. Rev. Lett.* **42** 518
[11] Frisch H L and Hammersley J M 1963 *J. Soc. Ind. Appl. Math.* **11** 894
[12] Agrawal P, Render S, Reynolds P J and Stanley H E 1979 *J. Phys. A: Math. Gen.* **12** 2073
[13] Nakanishi H and Reynolds P J 1979 *Phys. Lett.* **71A** 252
[14] Yanuka M and Englman R 1990 *J. Phys. A: Math. Gen.* **23** L339
[15] Tarasevich Y Y and van der Marck S C 1999 *Int. J. Mod. Phys.* C **10** 1193
[16] Ziff R M and Gu H 2009 *Phys. Rev.* E **79** 020102
[17] Nduwayo L, Lindebaum R and Chetty N 2009 *Comput. Phys. Commun.* **180** 503
[18] Tsallis C and de Magalhães A C N 1996 *Phys. Rep.* **268** 305
[19] Dolz M, Nieto F and Ramirez-Pastor A J 2005 *Phys. Rev.* E **72** 066129
[20] González M I, Centres P M, Lebrecht W, Ramirez-Pastor A J and Nieto F 2013 *Physica* A **392** 6330
[21] Yonezawa F, Sakamoto S and Hori M 1989 *Phys. Rev.* B **40** 636
Yonezawa F, Sakamoto S and Hori M 1989 *Phys. Rev.* B **40** 650
[22] Binder K 1997 *Rep. Prog. Phys.* **60** 488
[23] Lebrecht W, Valdés J F, Vogel E E, Nieto F and Ramirez-Pastor A J 2013 *Physica* A **392** 149
[24] Lebrecht W, Valdés J F, Vogel E E, Nieto F and Ramirez-Pastor A J 2014 *Physica* A **398** 234
[25] Lebrecht W, Vogel E E, Valdés J F, Ramirez-Pastor A J, Centres P M, González M I and Nieto F 2015 *Phys. Rev.* E **92** 012129
[26] Hoshen J and Kopelman R 1976 *Phys. Rev.* B **14** 3438
Hoshen J, Kopelman R and Monberg E M 1978 *J. Stat. Phys.* **19** 219
[27] Makoto M and Takuji N 1998 *ACM Trans. Model. Comput. Simul.* **8** 3
[28] Newman M E J and Ziff R M 2001 *Phys. Rev.* E **64** 016706
[29] Lorenz C D and Ziff R M 1998 *Phys. Rev.* E **57** 230
[30] Ballesteros P N, Fernández L A, Martín-Mayor V, Muñoz Sudepe A, Parisi G and Ruiz-Lorenzo J J 1999 *J. Phys. A: Math. Gen.* **32** 1
[31] Wang J, Zhou Z, Zhang W, Garoni T M and Deng Y 2013 *Phys. Rev.* E **87** 052107
[32] Hu H, Blöte H W, Ziff R M and Deng Y 2014 *Phys. Rev.* E **90** 042106
[33] Xu X, Wang J, Lv J-P and Deng Y 2014 *Front. Phys.* **9** 113
[34] Tsallis C 2004 *Physica* A **344** 718
[35] Weinan E, Ren W and Vanden-Eijnden E 2002 *Phys. Rev.* B **66** 052301
[36] Weinan E, Ren W and Vanden-Eijnden E 2007 *J. Chem. Phys.* **126** 164103

J. Stat. Mech. (2016) 093210